

Cite this: *RSC Adv.*, 2017, 7, 15211

# Deoxygenation of coal bed methane on LaCoO<sub>3</sub> perovskite catalyst: the structure evolution and catalytic performance

Zhenyang Zhao,<sup>†</sup> Li Wang,<sup>†</sup> Jian Ma, Yafen Feng, Xiaoming Cao, Wangcheng Zhan, Yanglong Guo, Yun Guo<sup>\*</sup> and Guanzhong Lu

A series of perovskite-type LaBO<sub>3</sub> (B = Fe, Co, Mn, and Ni) materials have been studied as catalysts for coal bed methane (CBM) deoxygenation. Among them, LaCoO<sub>3</sub> shows the best catalytic performance and stability, O<sub>2</sub> could be completely eliminated by CH<sub>4</sub> to produce CO<sub>2</sub> and H<sub>2</sub>O in the range of 400–720 °C, and the complete deoxidization could be maintained at temperatures of 400, 500, 600, and 660 °C for 100 h. Furthermore, the structure of LaCoO<sub>3</sub> could transform from perovskite to Co/La<sub>2</sub>O<sub>3</sub> through La<sub>2</sub>CoO<sub>4</sub>/LaCoO<sub>3</sub> and La<sub>2</sub>CoO<sub>4</sub>/Co<sub>3</sub>O<sub>4</sub> during the process of CBM deoxygenation. The results of H<sub>2</sub>-TPR and O<sub>2</sub>-TPO showed the perovskite LaCoO<sub>3</sub> is like a smart catalyst, whereby the Co species could reversibly move into and out of the perovskite structure depending on the temperature and reaction atmosphere. When Co species exist in an oxidised state (Co<sub>3</sub>O<sub>4</sub>, La<sub>2</sub>CoO<sub>4</sub> and/or LaCoO<sub>3</sub>), the CH<sub>4</sub> in CBM is completely oxidized by O<sub>2</sub> to produce CO<sub>2</sub> and H<sub>2</sub>O, the results of isotopic tracer experiments and pulse reaction demonstrate that the reaction follows the Mars–van Krevelen mechanism. However, the preferred products of the CBM deoxygenation reaction are CO and H<sub>2</sub> on Co/La<sub>2</sub>O<sub>3</sub> through partial oxidation of CH<sub>4</sub>. With the structure transforming from Co/La<sub>2</sub>O<sub>3</sub> to LaCoO<sub>3</sub> after reoxidation by O<sub>2</sub>, the activity of CBM deoxygenation could be recovered.

Received 17th December 2016  
Accepted 13th February 2017

DOI: 10.1039/c6ra28339j

rsc.li/rsc-advances

## 1. Introduction

Coal bed methane (CBM), also known as coal mine gas, is a kind of flammable gas whose main component is methane.<sup>1</sup> The direct emission of CBM is not only a waste of energy, but also pollutes the environment, because the warming potential of CH<sub>4</sub> is over 20 times of CO<sub>2</sub> as a greenhouse gas.<sup>2</sup> At a typical gassy mine, CBM is mainly emitted in three streams: (1) gas drained from the steam before mining, containing 60–95 vol% CH<sub>4</sub> and inert gas, which could be directly used or easily used to produce pure CH<sub>4</sub>; (2) gas drained from the worked areas of the mine, *e.g.* goaf, containing 30–95 vol% CH<sub>4</sub> and some O<sub>2</sub> (2–6 vol%);<sup>3,4</sup> (3) CH<sub>4</sub> ventilation air (0.1–1 vol% CH<sub>4</sub>).<sup>5</sup>

For the utilization of CBM with high CH<sub>4</sub> concentration and low O<sub>2</sub> concentration, it is necessary to remove the O<sub>2</sub> from the mixture, because the existence of O<sub>2</sub> could be dangerous in the process of storage and transportation. Usually, two main methods are used in CBM deoxygenation: non-catalytic and catalytic deoxidization. The common non-catalytic methods include the adsorption of O<sub>2</sub>, coke burning and deep freezing

methods.<sup>6–8</sup> Compared with non-catalytic methods, the catalytic deoxygenation of CBM is a convenient and effective method to eliminate O<sub>2</sub> by catalytic combustion of CH<sub>4</sub>.<sup>9–11</sup> However, the catalytic combustion of CH<sub>4</sub> is a violent exothermal reaction with a huge  $\Delta H_{298}$  of  $-802.7 \text{ kJ mol}^{-1}$ , which could induce a severe temperature runaway of the reactor and sintering of the catalyst. Meanwhile, the high reaction temperature could cause CH<sub>4</sub> partial oxidation and a reforming reaction to produce CO and H<sub>2</sub> under the conditions of a large excess of CH<sub>4</sub>.<sup>12–14</sup> Therefore, a desirable catalyst used in catalytic deoxygenation of CBM should not only have high activity to remove O<sub>2</sub> at low temperatures, but also avoid the production of H<sub>2</sub> and CO through side reactions (partial oxidation, cracking and/or reforming reaction) across a wide temperature range.

Furthermore, the composition of the reaction gas in the CBM deoxidization reaction varies from aerobic conditions to reducing conditions with the consumption of O<sub>2</sub>, which requires the catalyst to maintain high performance under oxidizing and reducing conditions simultaneously. It is another challenge for the deoxygenation catalyst.

Supported noble metal catalysts are widely used in the catalytic combustion of CH<sub>4</sub>.<sup>15–20</sup> However, the excess CH<sub>4</sub> in the reaction gas would lead to particle oxidation or cracking reactions, and produce H<sub>2</sub> and CO at temperatures as low as 400 °C while providing high CH<sub>4</sub> conversion.<sup>21–26</sup> Lyubovsky *et al.*<sup>27</sup> prepared Al<sub>2</sub>O<sub>3</sub>-supported Pd, Pt and Ru catalysts for CH<sub>4</sub>

Key Laboratory for Advanced Materials and Research Institute of Industrial Catalysis, School of Chemistry & Molecular Engineering, East China University of Science and Technology, Shanghai 200237, People's Republic of China. E-mail: yunguo@ecust.edu.cn; Fax: +86 21 64253703; Tel: +86 21 64253703

<sup>†</sup> These authors contributed equally to this work.

oxidation under both fuel-rich and fuel-lean conditions. The partial oxidation products of  $H_2$  and CO appeared under fuel-rich conditions above the light-off temperature, and their concentration increased with increasing temperature. In addition, the chemical state change of the noble metal in the process of CBM deoxygenation could affect the activity of catalyst. Lu *et al.*<sup>28–30</sup> reported CBM deoxygenation on Pd–PdO–NiO/Ni-foam and found the oscillation of  $O_2$  conversion to be due to the formation of inert metal Pd under the reducing conditions. The presence of PdNi (alloy) induced by the *in situ* reaction could eliminate this  $O_2$  oscillation, and  $O_2$  completely oxidized  $CH_4$  to  $CO_2$  and  $H_2O$  in the temperature range of 350–500 °C.

Compared with the supported noble metal catalysts, transition metal oxide catalysts (such as Cu, Co Ni *etc.*) also have attracted great attention.<sup>31–33</sup> For example, Tao *et al.*<sup>34</sup> prepared a nano- $NiCo_2O_4$  catalyst *via* a co-precipitation method, which showed high activity for  $CH_4$  combustion under conditions of excess  $O_2$  in the temperature range of 350–550 °C due to the integration of nickel cations, cobalt cations and surface lattice oxygen atoms/oxygen vacancies at the atomic scale.

The perovskite-type oxides ( $ABO_3$ ) have high temperature stability in hydrocarbon ( $C_nH_{2n+2}$ ) oxidation<sup>35,36</sup> and reforming reactions.<sup>37,38</sup> For example,  $LaCoO_3$  and partially substituted  $LaCoO_3$  have been confirmed to have high activities and stabilities for the partial oxidation of  $CH_4$ .<sup>39–41</sup> Generally, perovskites prepared with La in the A position, and Co, Mn, Fe or Ni in position B, are used in the catalytic combustion of  $CH_4$ .<sup>42–45</sup> Meanwhile, the temperature of partial oxidation or reforming of  $CH_4$  over perovskite catalyst usually exceeds 600 °C, which is much higher than that of supported noble metal catalysts and the transition metal oxide catalysts.<sup>46,47</sup> For example, Slagtern and Olsbye<sup>48</sup> studied the partial oxidation of  $CH_4$  to syngas at 800 °C on La–M–O (M = Co, Ni, Rh, and Cr) perovskite catalysts, and found the main product was  $CO_2$  on La–Co–O with the main phase of  $LaCoO_3$ ,  $Co_3O_4$ , and  $La_2O_3$ .

Furthermore, the structure of perovskite-type oxides could be reversibly changed depending on the composition of the reaction atmosphere. Nishihata *et al.*<sup>49</sup> reported that  $LaFe_{0.57}Co_{0.38}Pd_{0.05}O_3$  exhibited high catalytic activity during long term ageing, and the Pd reversibly moved into and out of the perovskite lattice during the cycle between oxidative and reductive atmospheres. Hence, the perovskite type catalyst may be a good candidate as a catalyst for CBM deoxygenation, and may be able to remove  $O_2$  from the CBM *via*  $CH_4$  combustion at a relatively low temperature, and maintain total oxidation across a wide temperature range by prohibiting partial oxidation and other side reactions.

In this work, perovskite-type oxides  $LaBO_3$  (B = Co, Mn, Fe and Ni) were prepared, and the activity and stability of  $LaBO_3$  for CBM catalytic deoxygenation were investigated. The evolution of  $LaCoO_3$  perovskite structure in the reaction and reaction mechanism were also explored.

## 2. Experimental section

### 2.1 Catalyst preparation

The perovskite-type oxides ( $LaBO_3$ , B = Co, Mn, Fe and Ni) were prepared by the co-precipitation method. A stoichiometric

amount of metal nitrate mixture solution and sodium hydroxide solution were simultaneously dropped into a NaOH solution with pH of 9–10 under stirring at 60 °C. The pH value of the mixture solution was kept in the range of 9–10 during the whole precipitation process. The obtained precipitate was aged at 60 °C for 2 h. After being washed by deionized water to neutral pH, the precipitate was filtered and dried at 100 °C for 12 h then calcined in air at 750 °C for 3 h to obtain the  $LaBO_3$  catalysts. The BET surface areas of the prepared  $LaBO_3$  are in the range of 12 to 15  $m^2 g^{-1}$ .

### 2.2 Catalyst characterization

The powder X-ray diffraction patterns (XRD) of catalysts were obtained with a RigakuD/max 2550 VB/PC diffractometer with a Cu K $\alpha$  radiation ( $\lambda = 1.54056$ , scanning step 0.02°). Spectra were collected in a range of  $2\theta = 10$ –80° with a scanning rate of 6°  $min^{-1}$ . In order to obtain more details about the structure of the sample after reduction, the mapping of the elements was measured on the JOEL 2100 instrument operating at 200 kV.

The X-ray photoelectron spectroscopy (XPS) spectra were recorded on an AXIS-Ultra-DLD spectrometer with a Al K $\alpha$  X-ray source (1486.6 eV). The base pressure inside the analysis chamber was  $3 \times 10^{-10}$  Torr. The XPS spectra of the selected elements were measured with the constant analyzer pass energy of 40 eV. All binding energies (BE) were referenced to the adventitious C 1s peak (BE = 284.8 eV).

The specific surface areas of the catalysts were measured using the  $N_2$  adsorption isotherm at –196 °C by using an automatic Micromeritics ASAP 2020 analyzer.

The temperature-programmed reduction of  $H_2$  ( $H_2$ -TPR) experiments were carried out by a conventional flow system equipped with a thermal conductivity detector (TCD). 100 mg catalyst was calcined at 400 °C for 1 h in air before the TPR reaction, and then cooled to room temperature. The pretreated catalyst was heated in a flow of 5 vol%  $H_2/N_2$  (45  $mL min^{-1}$ ) at a heating rate of 10 °C  $min^{-1}$  from room temperature to 800 °C. After  $H_2$ -TPR, the catalyst was maintained at 800 °C for 1 h in a flow of 5 vol%  $H_2/N_2$  (45  $mL min^{-1}$ ), then purged with pure He for 1 h. After cooling to room temperature in a He flow, the temperature programmed oxidation of  $O_2$  ( $O_2$ -TPO) was performed using the same apparatus; 1 vol%  $O_2/He$  (50  $mL min^{-1}$ ) was used in  $O_2$ -TPO, and the composition of the outlet gas was monitored by an on-line quadrupole mass spectrometer (IPC 400, INFICON Co. Ltd.).

Isotope tracer experiments were conducted in the quartz tube reactor and the effluent gas was monitored by an on-line quadrupole mass spectrometer (MS, IPC 400, INFICON Co. Ltd.).

The catalyst was pretreated at 700 °C for 2.5 h in pure He at 50  $mL min^{-1}$ . 500 mg catalyst was used in the pulse experiments, 517.3  $\mu L$  of 12 vol%  $^{18}O_2/6$  vol%  $CH_4$  was pulsed into the reactor 20 times. 200 mg catalyst was used in the continuous isotope tracer experiments at different designated temperatures, 12 vol%  $^{18}O_2/6$  vol%  $CH_4$  was used as the reaction gas.

The reaction orders of  $O_2$  and  $CH_4$  were measured in the temperature range of 340 to 410 °C with feed steams of 4.0–12.0



kPa O<sub>2</sub>, CH<sub>4</sub> and N<sub>2</sub>. 1.0 kPa CH<sub>4</sub> was used to investigate the catalytic combustion of CH<sub>4</sub>, and 50.0 kPa CH<sub>4</sub> was used in the deoxygenation of CBM. The O<sub>2</sub>/CH<sub>4</sub> conversion was adjusted to below 15% by varying the space velocity in the range of 6000–72 000 mL g<sup>−1</sup> h<sup>−1</sup> so as to eliminate the thermal effect and diffusion effect.

CH<sub>4</sub> and O<sub>2</sub> pulse experiments were conducted on the same apparatus as that for the isotope tracer experiments. The procedures were as follows: (1) 10 vol% CH<sub>4</sub>/He was pulsed into 500 mg catalyst 20 times (CH<sub>4</sub>-1st); (2) 20 pulses of pure O<sub>2</sub> was passed through the catalyst bed; (3) step 1 was repeated again (CH<sub>4</sub>-2nd). The pulse volume was 517.3 μL.

### 2.3 Evaluation of the catalytic performance

The catalytic activities of LaBO<sub>3</sub> (B = Co, Mn, Fe and Ni) catalysts for the simulated deoxygenation of CBM were tested in a fixed bed quartz tubular reactor at atmospheric pressure, 300 mg catalyst (40–60 mesh) diluted with 2 g silica sand (20–40 mesh) was used. The feed gas, containing 50 vol% CH<sub>4</sub>, 6 vol% O<sub>2</sub> and N<sub>2</sub> to balance, was passed through the catalytic bed at a flow rate of 30 mL min<sup>−1</sup>. The temperature of the catalyst bed was measured by a thermocouple inserted in the top of the catalyst bed, and the heating rate was 4 °C min<sup>−1</sup>. An on-line gas chromatograph (Agilent 7890) was used to monitor the composition of the outlet gas. The catalyst activity was expressed by *T*<sub>10</sub> and *T*<sub>90</sub> of O<sub>2</sub>, which corresponded to the reaction temperatures required for 10% and 90% O<sub>2</sub> conversion, respectively.

Because the excess CH<sub>4</sub> in the feed gas could lead to partial oxidation or the reforming reaction to produce CO and H<sub>2</sub> at high temperature, the temperature range between the lowest temperature of complete conversion (LTCC) of O<sub>2</sub> and the initial temperature of H<sub>2</sub> formation is defined as the operation window of the catalyst for the deoxygenation reaction.

## 3. Results

### 3.1 Catalytic activities of LaBO<sub>3</sub>

The catalytic activities of LaBO<sub>3</sub> (B = Co, Fe, Mn and Ni) for CBM deoxygenation are shown in Fig. 1. The type of transition metal in the B-site shows a significant effect on the catalytic activity of the perovskites. LaFeO<sub>3</sub> shows the lowest activity for O<sub>2</sub> elimination, *T*<sub>10</sub> and *T*<sub>90</sub> are 350 and 450 °C, respectively. Meanwhile, LaCoO<sub>3</sub> exhibits the highest catalytic activity, the *T*<sub>10</sub> and *T*<sub>90</sub> are 300 and 390 °C, respectively. Combined with the results of the BET surface area in Table 1, the activity of the catalyst is not directly related to its surface area.

The excess CH<sub>4</sub> in the feed gas could produce H<sub>2</sub> and CO by the partial oxidation or reforming reaction at high reaction temperature (>700 °C). The production of H<sub>2</sub> following the reaction temperature in CBM deoxygenation on different catalysts is shown in Fig. 1b. CO was observed simultaneously but is not shown. The results in Fig. 1b show the initial sequence of H<sub>2</sub> formation is LaFeO<sub>3</sub> < LaMnO<sub>3</sub> < LaNiO<sub>3</sub> < LaCoO<sub>3</sub>, and the H<sub>2</sub> formation on LaNiO<sub>3</sub> increases more rapidly than the others when the temperature exceeds 700 °C. Combined with the

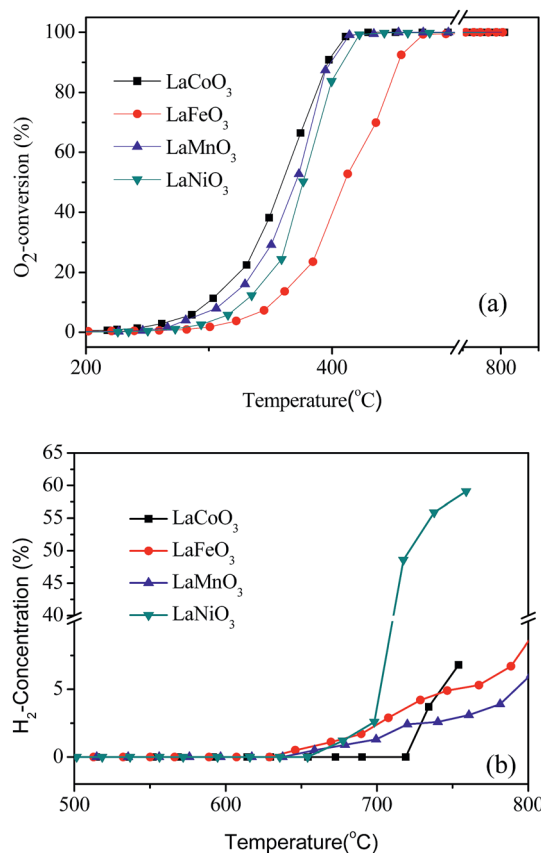


Fig. 1 The conversion of O<sub>2</sub> (a) and production of H<sub>2</sub> (b) in the deoxygenation reaction by LaBO<sub>3</sub> catalysts as a function of temperature.

results in Fig. 1a, LaCoO<sub>3</sub> shows the widest operation window, where O<sub>2</sub> could be completely eliminated by CH<sub>4</sub> in the temperature range of 400 to 720 °C. Continuously increasing the reaction temperature, the amount of H<sub>2</sub> and CO increased rapidly. Therefore, catalyst LaCoO<sub>3</sub> was selected for the further investigation in the following sections.

The stability of LaCoO<sub>3</sub> for deoxygenation reaction was investigated at temperatures of 360, 400, 500, 600, and 660 °C for 100 h. The results in Fig. 2 show O<sub>2</sub> conversion was maintained at 360 °C at about 75% for 100 h, and O<sub>2</sub> could be completely eliminated at 400 and 660 °C for 100 h, and H<sub>2</sub> and CO were not detected during the whole experiments. The same results were obtained at 500 and 600 °C, which are not shown. After reaction at 660 °C for 100 h, the light-off activity of the aged catalyst is nearly consistent with the fresh one (Fig. 2b), which indicates that LaCoO<sub>3</sub> has high stability for the deoxygenation reaction in the temperature range of 400–660 °C.

### 3.2 XRD

The XRD patterns of the fresh LaBO<sub>3</sub> catalysts are exhibited in Fig. 3. The prepared LaBO<sub>3</sub> (Ni, Mn and Co) show a typical hexagonal perovskite structure. For catalyst LaFeO<sub>3</sub>, the major phase is orthorhombic perovskite structure, and some weak diffraction peaks corresponding to Fe<sub>2</sub>O<sub>3</sub> and La<sub>2</sub>O<sub>3</sub> are also



**Table 1** The cell parameters<sup>a</sup>, crystallite size<sup>b</sup> and BET area of the perovskites

	LaCoO <sub>3</sub>	LaFeO <sub>3</sub>	LaMnO <sub>3</sub>	LaNiO <sub>3</sub>
Spatial group	Hexagonal	Orthorhombic	Hexagonal	Hexagonal
<i>a</i> (Å)	5.4358	5.4672	6.0731	5.5953
<i>b</i> (Å)	5.4358	6.7968	6.0731	5.5953
<i>c</i> (Å)	13.0643	28.8799	13.4010	5.6679
Crystallite size (nm)	39.1	53.72	10.7	26.4
BET area (m <sup>2</sup> g <sup>-1</sup> )	11	16	22	14

<sup>a</sup> The cell parameters were obtained by Rietveld refinement calculations from the diffractogram of the structures. <sup>b</sup> The crystallite size was calculated by the Debye-Scherrer formula.

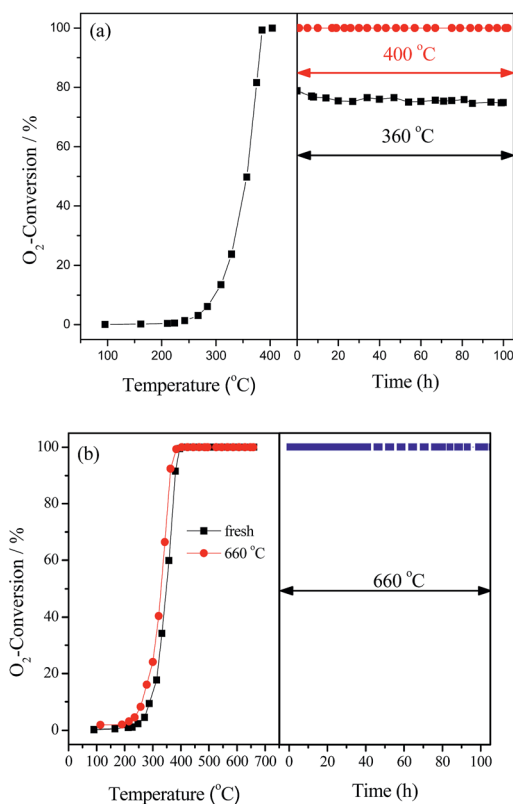


**Fig. 2** The stability of LaCoO<sub>3</sub> measured at 360, 400 °C (a) and 660 °C (b). In part (b) the catalytic activity of fresh LaCoO<sub>3</sub> (■) and after reaction at 660 °C for 100 h (●) are compared.

detected at  $2\theta = 33, 35, 49$  and  $54^\circ$  and  $2\theta = 26, 30, 39$  and  $52^\circ$ , respectively. The cell parameters, crystallite size and BET surface area of the perovskites are listed in Table 1.

Fig. 4 shows the XRD patterns of LaCoO<sub>3</sub> after stability tests at different temperatures. Compared with the results in Fig. 3, there is no observable difference in the LaCoO<sub>3</sub> structure after reaction at 400 and 500 °C for 100 h (Fig. 4a and b), which indicates the stability of the perovskite structure. However, after reaction at 600 °C for 100 h (Fig. 4c), the structure of LaCoO<sub>3</sub> transforms from perovskite into a mixture of perovskite (LaCoO<sub>3</sub>,  $2\theta = 23, 33, 40, 53$  and  $59^\circ$ ) and perovskite-like (La<sub>2</sub>CoO<sub>4</sub>,  $2\theta = 24, 32, 43, 47$  and  $65^\circ$ ). Continuously increasing the reaction temperature to 660 °C, only perovskite-like La<sub>2</sub>CoO<sub>4</sub> and Co<sub>3</sub>O<sub>4</sub> crystal phases are detected after 100 h

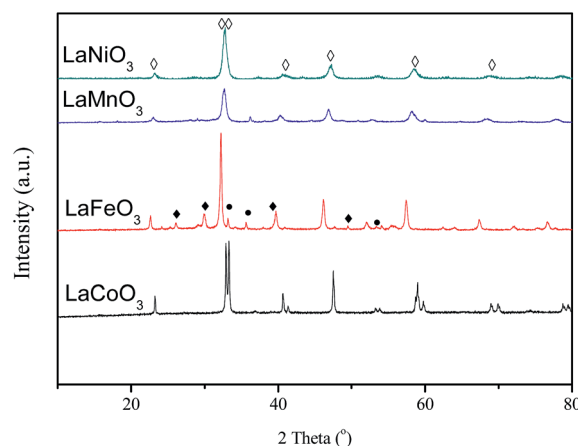


**Fig. 3** XRD patterns of LaBO<sub>3</sub> (◇: perovskite; ●: Fe<sub>2</sub>O<sub>3</sub>; ◆: La<sub>2</sub>O<sub>3</sub>).

reaction (Fig. 4d). Combined with the results in Fig. 2, it could be concluded that the structure change of LaCoO<sub>3</sub> is dependent on the reaction temperature, but this structure evolution does not bring an apparent difference in the catalytic performance of LaCoO<sub>3</sub> for CBM deoxygenation.

When the deoxygenation reaction is finished at 800 °C, the perovskite structure of LaCoO<sub>3</sub> is completely destroyed, and only La<sub>2</sub>O<sub>3</sub> is detected at  $2\theta = 26, 30, 39$  and  $52^\circ$  (Fig. 4e). The results

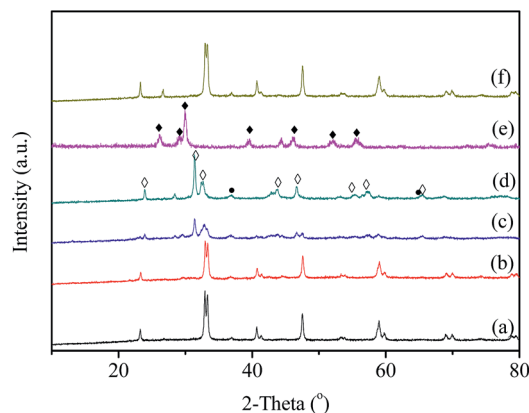


**Fig. 4** The XRD patterns of the LaCoO<sub>3</sub> after reaction at 400 (a), 500 (b), 600 (c), and 660 °C (d) for 100 h and 800 °C (e), the re-oxidation of sample (e) at 750 °C in air (f) (◇: La<sub>2</sub>CoO<sub>4</sub>; ●: Co<sub>3</sub>O<sub>4</sub>; ◆: La<sub>2</sub>O<sub>3</sub>).





in Fig. 1 show the production of  $\text{H}_2$  and CO when the reaction temperature was higher than  $720^\circ\text{C}$ , which could lead to the reduction of  $\text{LaCoO}_3$ .<sup>46</sup> The diffraction peaks of Co species cannot be observed, which means Co species are highly dispersed or below the detection limit of XRD. However, it is worth noting that the completely destroyed  $\text{LaCoO}_3$  could be reverted back to the perovskite structure after reoxidation at  $750^\circ\text{C}$  in air (Fig. 4f).

### 3.3 XPS characterization

XPS characterization is performed to investigate the surface chemical state of the catalysts. Fig. 5 shows the Co 2p spectra of  $\text{LaCoO}_3$  after reaction at different temperatures (400, 500, 600, and  $660^\circ\text{C}$ ) for 100 h. The resolution of the asymmetrical spectra of Co 2p shows the co-existence of two species at BE of 779.8 and  $782.1\text{ eV}$ , which could be ascribable to  $\text{Co}^{3+}$  and  $\text{Co}^{2+}$ , respectively.<sup>50,51</sup>

The surface  $\text{Co}^{2+}/\text{Co}^{3+}$  ratio of  $\text{LaCoO}_3$  after reaction is much higher than that of fresh catalyst, and the  $\text{Co}^{2+}/\text{Co}^{3+}$  ratio increases with the increase in the reaction temperature as shown in Table 2, which indicates the partial reduction of  $\text{LaCoO}_3$  during the reaction, and coincides with the results of XRD shown in Fig. 4. The predominant crystal phase changes from perovskite to a mixture of  $\text{La}_2\text{CoO}_4$  and  $\text{Co}_3\text{O}_4$  through the mixed phase of  $\text{LaCoO}_3$  and  $\text{La}_2\text{CoO}_4$ , the average chemical state of the surface Co species is gradually reduced during this process.

### 3.4 Temperature programmed reaction

In order to further investigate the effects of reaction gas and temperature on structure evolution of  $\text{LaCoO}_3$  during the reaction, experiments of  $\text{H}_2$ -TPR and  $\text{O}_2$ -TPO are carried out.

The  $\text{H}_2$ -TPR profile of fresh  $\text{LaCoO}_3$  shows three reduction peaks in Fig. 6a. The peaks in the temperature range of  $200\text{--}500^\circ\text{C}$  correspond to the reduction of the oxygen adsorbed on the catalyst surface and reduction of  $\text{Co}^{3+}$  to  $\text{Co}^{2+}$ , the high temperature peak at  $500\text{--}800^\circ\text{C}$  could be assigned to the reduction of  $\text{Co}^{2+}$  to Co.<sup>46,52,53</sup> The XRD pattern of Fig. 7a demonstrates that the perovskite structure of  $\text{LaCoO}_3$  has been completely destroyed and converted to a mixture of metallic Co

**Table 2** The surface oxygen content (%) and  $\text{Co}^{2+}/\text{Co}^{3+}$  ratio of  $\text{LaCoO}_3$  obtained by XPS analysis

Sample <sup>a</sup>	Surface oxygen content (%)	$\text{Co}^{2+}/\text{Co}^{3+}$
Fresh	56.75	0.48
$400^\circ\text{C}$	53.72	0.83
$500^\circ\text{C}$	49.00	1.26
$600^\circ\text{C}$	49.23	3.29
$660^\circ\text{C}$	52.68	3.59

<sup>a</sup> After the stability test at specified temperature for 100 h.

and  $\text{La}_2\text{O}_3$  after  $\text{H}_2$ -TPR, which coincides with that of  $\text{LaCoO}_3$  after reaction at  $800^\circ\text{C}$  (Fig. 4).

After  $\text{H}_2$ -TPR,  $\text{O}_2$ -TPO of the reduced sample is performed. The result in Fig. 6b shows there are two  $\text{O}_2$  consumption peaks: a significant peak is located at the range of  $200\text{--}300^\circ\text{C}$  and a weak peak is observed at near  $700^\circ\text{C}$ .

For the sample after  $\text{H}_2$ -TPR, XRD results show that the main phases are  $\text{Co}_3\text{O}_4$  and  $\text{La}_2\text{O}_3$  after reoxidation at  $300^\circ\text{C}$  for 0.5 h (Fig. 7b), which indicates the  $\text{O}_2$  consumption peak at range of  $200\text{--}300^\circ\text{C}$  in Fig. 6b should correspond to the oxidation of metal Co to  $\text{Co}_3\text{O}_4$  ( $\text{Co}/\text{La}_2\text{O}_3 + \text{O}_2 \rightarrow \text{Co}_3\text{O}_4 + \text{La}_2\text{O}_3$ ). Because the oxidation of metal Co is a strong exothermic reaction, the accumulated heat could result in the direct oxidation of some metallic Co species to  $\text{Co}^{3+}$ . When the oxidation temperature is increased to  $750^\circ\text{C}$ , the perovskite structure of  $\text{LaCoO}_3$  was recovered ( $\text{Co}_3\text{O}_4 + \text{La}_2\text{O}_3 + \text{O}_2 \rightarrow \text{LaCoO}_3$ ), the main phase of

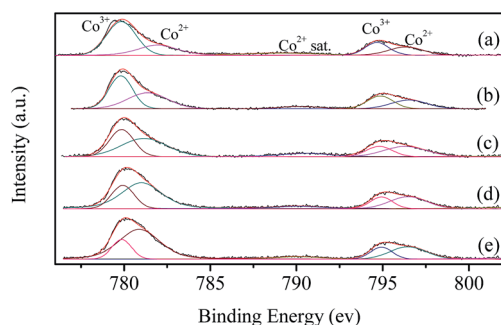


**Fig. 5** XPS spectra of fresh  $\text{LaCoO}_3$  (a) and aged  $\text{LaCoO}_3$  after stability tests at temperatures of  $400$  (b),  $500$  (c),  $600$  (d) and  $660^\circ\text{C}$  (e) for 100 h.

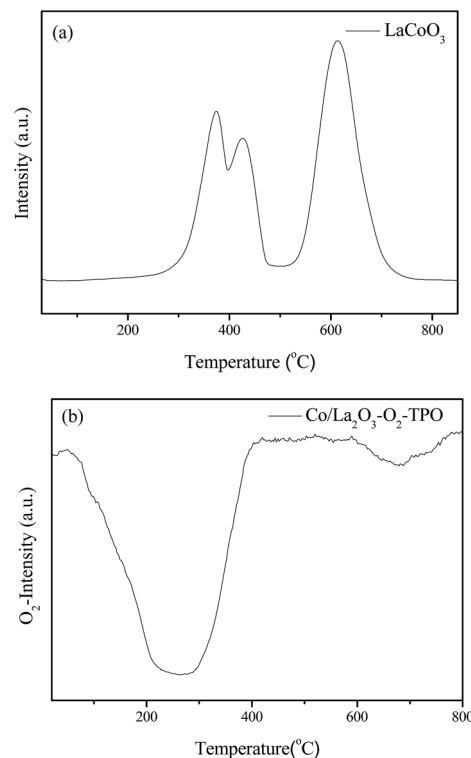


**Fig. 6**  $\text{H}_2$ -TPR (a) and  $\text{O}_2$ -TPO (b) profiles of  $\text{LaCoO}_3$ .



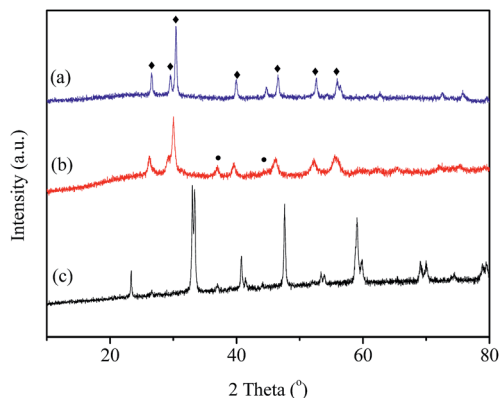


Fig. 7 (a) XRD patterns of  $\text{LaCoO}_3$  reduced by  $\text{H}_2$  at 800 °C (a); reoxidation by  $\text{O}_2$  at 300 °C (b) and 750 °C (c).  $\bullet$ ,  $\text{Co}_3\text{O}_4$ ;  $\blacklozenge$ ,  $\text{La}_2\text{O}_3$ .

the sample is perovskite with a minor  $\text{Co}_3\text{O}_4$  phase observed at  $2\theta = 37^\circ$  (Fig. 7c), which corresponds to the  $\text{O}_2$  consumption at the high temperature range in Fig. 6b.

### 3.5 Kinetic analysis

Fig. 8 shows the pressure-dependent reaction rates on the partial pressure of  $\text{O}_2$  ( $P_{\text{O}_2}$ ) from 4.0 to 12.0 kPa while keeping

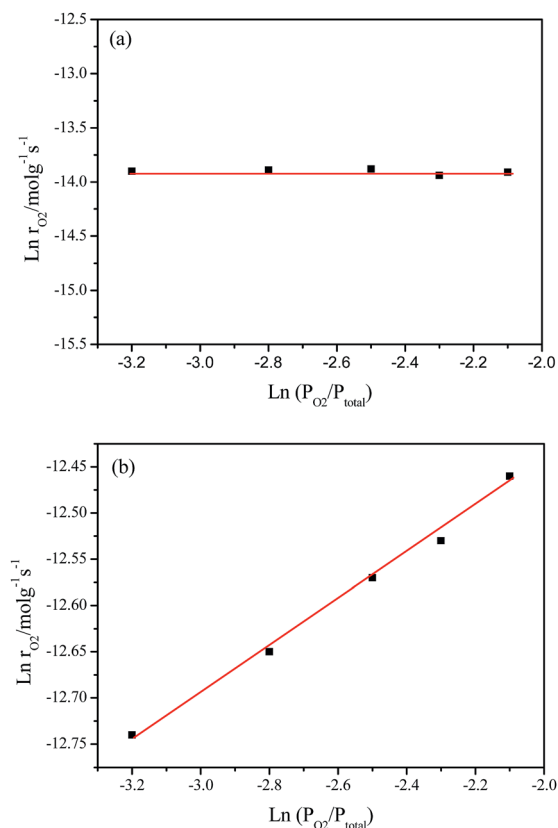


Fig. 8  $\ln r_{\text{O}_2}$  as a function of  $\ln P_{\text{O}_2}$  over  $\text{LaCoO}_3$ : (a) at 420 °C, the feed gas consisted of 4–12%  $\text{O}_2$  and 1%  $\text{CH}_4$  at a space velocity of 30 000  $\text{mL g}^{-1} \text{h}^{-1}$ ; (b) at 370 °C, the feed gas consisted of 4–12%  $\text{O}_2$  and 50%  $\text{CH}_4$  at a space velocity of 48 000  $\text{mL g}^{-1} \text{h}^{-1}$ .

the partial pressure of  $\text{CH}_4$  ( $P_{\text{CH}_4}$ ) at 1.0 to 50.0 kPa, which corresponds to the catalytic combustion of  $\text{CH}_4$  and deoxygenation of CBM, respectively.

Under  $\text{O}_2$  rich conditions, the  $\text{O}_2$  reaction rate doesn't change with an increase in  $P_{\text{O}_2}$ , yielding an order of 0 with respect to  $\text{O}_2$  at 420 °C. The fact that reaction order of  $\text{O}_2$  is about zero shows the  $\text{O}_2$  concentration hardly affect the rate of  $\text{O}_2$  consumption, which implies the activation of  $\text{CH}_4$  is the rate determination step for  $\text{CH}_4$  combustion under  $\text{O}_2$  excess.<sup>54,55</sup>

However, under oxygen lean conditions, the  $\text{O}_2$  reaction rates increases with an increase in  $P_{\text{O}_2}$ , yielding an order of 0.25 with respect to  $\text{O}_2$  at 370 °C, which demonstrates that the activation of  $\text{O}_2$  is a key factor for CBM deoxygenation reaction. The apparent activation energy ( $E_a$ ) of deoxygenation reaction on  $\text{LaCoO}_3$  is 121  $\text{kJ mol}^{-1}$ , as shown in Fig. 9.

### 3.6 Isotopic tracer experiments

The isotopic tracer pulse reaction results of  $^{18}\text{O}_2 + \text{CH}_4$  are shown in Fig. 10. When the temperature is 600 °C,  $^{18}\text{O}_2$  ( $\text{O}_2\text{-}36$ ) is completely consumed in the 20 pulses on the  $\text{LaCoO}_3$  (Fig. 10a), and the production of  $\text{C}^{16}\text{O}_2$  ( $m/z = 44$ ) could be observed at the same time. Furthermore, any  $\text{CO}_2$  containing  $^{18}\text{O}$  ( $m/z = 46$  and 48) are not detected, which indicates  $\text{CH}_4$  reacts with the lattice oxygen rather than gas  $^{18}\text{O}_2$ . The same results are obtained at the temperature of 700 °C (Fig. 10b).

When the feed gas of 12 vol%  $^{18}\text{O}_2$ /6 vol%  $\text{CH}_4$  continuously passes through the catalyst bed at 600 °C, the result in Fig. 11a shows that  $\text{C}^{16}\text{O}_2$  is produced immediately and exists as the dominant product in the first 300 s, then the content of  $\text{C}^{16}\text{O}_2$  obviously decreases with the increase of reaction time. Meanwhile, the content of  $\text{C}^{16}\text{O}^{18}\text{O}$  (46) and  $\text{C}^{18}\text{O}_2$  (48) increases gradually. After 40 min,  $\text{C}^{18}\text{O}_2$  becomes the main product, next is  $\text{C}^{16}\text{O}^{18}\text{O}$ . Similar results are obtained at 700 °C, as shown in Fig. 11b. Combined with the results in Fig. 10, it may be suggested that the deoxidization reaction of CBM may follow the Mars–van Krevelen mechanism: the  $\text{CH}_4$  in the feed gas firstly reacts with lattice oxygen and creates oxygen vacancies, which could be replenished by the diffusion of lattice oxygen from bulk to surface and the adsorption and activation of gas  $\text{O}_2$ .

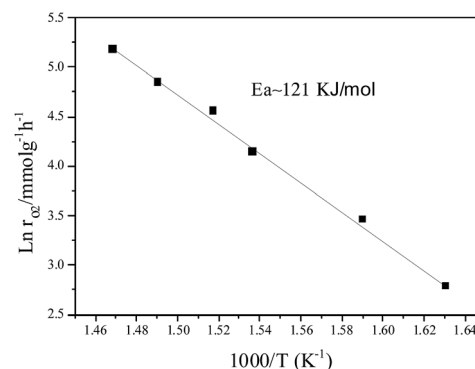


Fig. 9 Arrhenius plot of the reaction rate ( $\ln r$ ) vs.  $1/T$  for  $\text{O}_2$  deoxygenation over  $\text{LaCoO}_3$ .



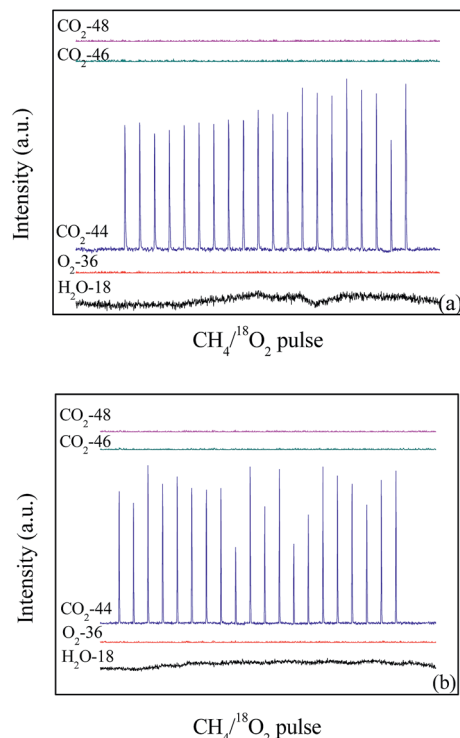


Fig. 10 The pulses test of catalyst LaCoO<sub>3</sub> under the conditions of 12 vol% <sup>18</sup>O<sub>2</sub>/6 vol% CH<sub>4</sub> at 600 (a) and 700 °C (b).

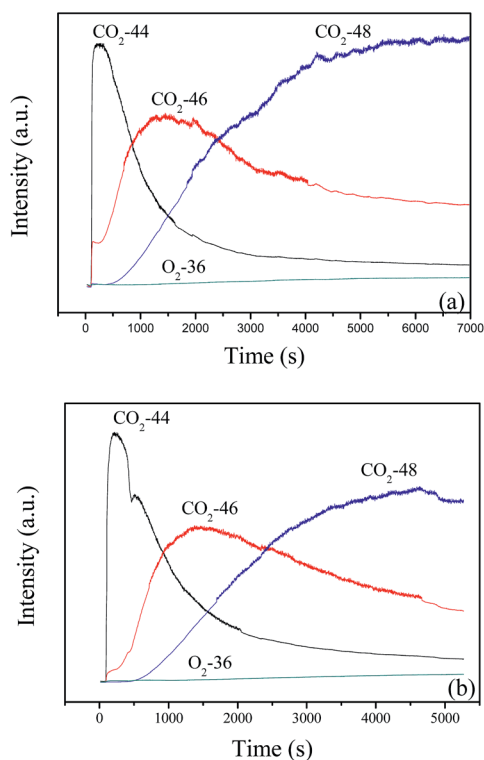


Fig. 11 The continuous reaction of 12 vol% <sup>18</sup>O<sub>2</sub>/6 vol% CH<sub>4</sub> balanced with N<sub>2</sub> on LaCoO<sub>3</sub> at 600 (a) and 700 °C (b).

### 3.7 Pulse reaction

The results in Fig. 4 showed structure transformation of LaCoO<sub>3</sub> during the CBM deoxygenation reaction. Separated CH<sub>4</sub> and O<sub>2</sub> pulse reactions on LaCoO<sub>3</sub> and pre-reduced LaCoO<sub>3</sub> at different temperatures are performed to explore the effects of LaCoO<sub>3</sub> structure on the CBM deoxygenation reaction and the formation mechanism of byproducts (H<sub>2</sub> and CO); the results are shown in Fig. 12 and 13.

For the CH<sub>4</sub> pulse reaction on LaCoO<sub>3</sub> at 700 °C (CH<sub>4</sub>-1st, Fig. 12a), most of the CH<sub>4</sub> is consumed in 20 pulses, accompanied by the production of CO<sub>2</sub> and H<sub>2</sub>O simultaneously. At the same time, weak signals of CO (*m/z* = 28) are also detected. Based on the standard spectra of CO<sub>2</sub>, the CO signals may be induced by dissociative ionisation of CO<sub>2</sub> in the chamber of mass spectrometer. After the CH<sub>4</sub> pulses, 20 pulses of O<sub>2</sub> were passed through catalyst bed, CO<sub>2</sub>/CO and H<sub>2</sub>O were not detected during this process (not shown).

For the second run of CH<sub>4</sub> pulse reactions (CH<sub>4</sub>-2nd, Fig. 12b), the similar results to those in CH<sub>4</sub>-1st are obtained, which indicates CH<sub>4</sub> is oxidized by the lattice and/or adsorbed oxygen on LaCoO<sub>3</sub> to produce CO<sub>2</sub> and H<sub>2</sub>O, but insufficient lattice oxygen or limited diffusion rate of lattice oxygen from bulk to surface leads to the residual CH<sub>4</sub>.

The signals of CO (*m/z* = 28) in the pulse reaction are induced by the dissociative ionisation of CO<sub>2</sub> in the chamber of mass spectrometer, while not from the reaction production. We have already explained this phenomenon in the CH<sub>4</sub> pulse reaction on LaCoO<sub>3</sub> at 700 °C. However, the results in Fig. 1 show the production of CO and H<sub>2</sub> in the deoxidization reaction when the temperature is higher than 720 °C. It should be noted that the structure of the perovskite LaCoO<sub>3</sub> transforms to Co/La<sub>2</sub>O<sub>3</sub> in the deoxidization reaction at a temperature higher than 720 °C (Fig. 4).

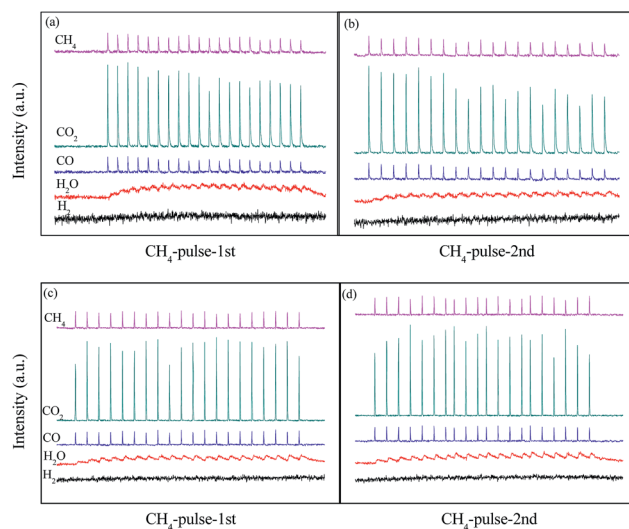


Fig. 12 CH<sub>4</sub> pulse reaction at 700 (a, b) and 800 °C (c, d) on LaCoO<sub>3</sub> (a and c are the first run of CH<sub>4</sub> pulse reaction, b and d are the second run).



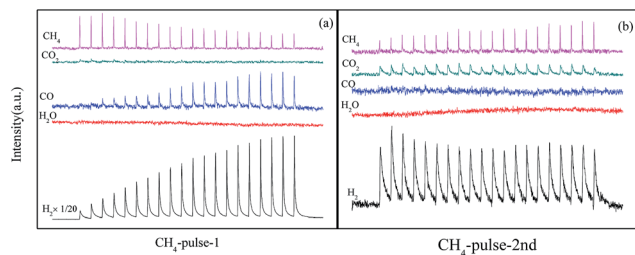


Fig. 13 CH<sub>4</sub> pulse reaction on Co/La<sub>2</sub>O<sub>3</sub> at 700 °C (a: first run, b: second run).

In order to further investigate CBM deoxygenation reaction on Co/La<sub>2</sub>O<sub>3</sub>, the LaCoO<sub>3</sub> with perovskite structure is pretreated with 10% H<sub>2</sub>/N<sub>2</sub> at 800 °C to obtain Co/La<sub>2</sub>O<sub>3</sub> (Fig. 7), then the pulse reactions are performed after purging with He for 0.5 h. In the first run of CH<sub>4</sub> pulse reaction on Co/La<sub>2</sub>O<sub>3</sub> at 700 °C (Fig. 13a), most of the CH<sub>4</sub> is consumed while H<sub>2</sub> and CO is generated, and the amount of H<sub>2</sub> and CO significantly increases with an increase in the number of pulses. Meanwhile, a trace amount of CO<sub>2</sub> is detected at the beginning of the pulse reaction, and the amount of CO<sub>2</sub> decreases gradually. After 3 pulses, the CO<sub>2</sub> could hardly be detected.

During the following O<sub>2</sub> pulse reaction, O<sub>2</sub> is completely consumed in the 20 pulses due to the oxidation of Co/La<sub>2</sub>O<sub>3</sub>. CO/CO<sub>2</sub>, H<sub>2</sub> and H<sub>2</sub>O are not observed during this process, the results are not shown.

After the O<sub>2</sub> pulse reaction, the second run of the CH<sub>4</sub> pulse reaction (CH<sub>4</sub>-2nd) is performed. Fig. 13b shows the production of CO<sub>2</sub>, CO and H<sub>2</sub>, and their amount remains nearly constant during the 20 pulses, which is significantly different from the results in Fig. 13a. It may be induced by the partial Co/La<sub>2</sub>O<sub>3</sub> oxidation to CoO<sub>x</sub>/La<sub>2</sub>O<sub>3</sub> by O<sub>2</sub> during the process of the O<sub>2</sub> pulse reaction. The formation of CoO<sub>x</sub>/La<sub>2</sub>O<sub>3</sub> decreases the amount of Co/La<sub>2</sub>O<sub>3</sub>, which leads to the significant decrease of CO and H<sub>2</sub>.

## 4. Discussion

The results in Fig. 1 and 2 show LaCoO<sub>3</sub> behaves with high activity and stability for CBM deoxygenation across a wide temperature range, O<sub>2</sub> could be completely eliminated by CH<sub>4</sub> to produce CO<sub>2</sub> and H<sub>2</sub>O in the range of 400–720 °C, and the activity of LaCoO<sub>3</sub> could be maintained after reaction at 400, 500, 600 or 660 °C for 100 h.

Roseno *et al.*<sup>39</sup> investigated the structure change of LaCoO<sub>3</sub> in partial oxidation of CH<sub>4</sub>, and found that high temperature reduction could decompose the perovskite structure of LaCoO<sub>3</sub> to Co/La<sub>2</sub>O<sub>3</sub>, and metallic Co was oxidized to CoO in O<sub>2</sub>, and further reacted with La<sub>2</sub>O<sub>3</sub> to form La<sub>2</sub>CoO<sub>4</sub> with spinel structure. During CBM deoxidization reaction, the structure of LaCoO<sub>3</sub> gradually transfers from perovskite to Co/La<sub>2</sub>O<sub>3</sub> depending on the reaction temperature (Fig. 4). The H<sub>2</sub>-TPR also showed the structure evolution of LaCoO<sub>3</sub> induced by the reduction of H<sub>2</sub> in the feed gas. Meanwhile, the destructed perovskite structure could be recovered from Co/La<sub>2</sub>O<sub>3</sub> by

calcination or reoxidation (Fig. 4 and 7). The structure evolution of LaCoO<sub>3</sub> depending on the temperature and reaction gas is shown schematically in Fig. 14, which demonstrates that Co species could reversibly move into and out of the perovskite structure depending on the temperature and reaction atmosphere.

Based on the results in Fig. 7, the LaCoO<sub>3</sub> has been reduced by 5 vol% H<sub>2</sub>/N<sub>2</sub> (45 mL min<sup>-1</sup>) at 750 °C for 30 min to obtain Co/La<sub>2</sub>O<sub>3</sub> (LaCoO<sub>3</sub>-R), then Co/La<sub>2</sub>O<sub>3</sub> is reoxidized to perovskite LaCoO<sub>3</sub> (LaCoO<sub>3</sub>-R-O). The activities of CBM deoxygenation in Fig. 15 show that LaCoO<sub>3</sub>-R behaves with much higher activity than LaCoO<sub>3</sub>-R-O, and there are no by-products of CO and H<sub>2</sub> before 720 °C, as with LaCoO<sub>3</sub>-R-O. Compared with the result in Fig. 1, LaCoO<sub>3</sub>-R-O shows nearly the same activity as fresh LaCoO<sub>3</sub>. Combined with the results in Fig. 6 and 7, the apparently enhanced activity of LaCoO<sub>3</sub>-R in the low temperature range may be derived from the oxidation of metallic Co by O<sub>2</sub>. The above results indicate that even if the structure of LaCoO<sub>3</sub> with perovskite is completely destroyed when the CBM deoxygenation temperature exceeds 720 °C, the structure and activity could be recovered after calcination at 750 °C in O<sub>2</sub>. Therefore, LaCoO<sub>3</sub> like a smart catalyst, its structure could be reversibly transformed between Co/La<sub>2</sub>O<sub>3</sub>, La<sub>2</sub>CoO<sub>4</sub> and LaCoO<sub>3</sub> depending on the temperature and reaction atmosphere. This reversible structure evolution of LaCoO<sub>3</sub> could meet the challenge of the shift between oxidative and reductive atmosphere typically encountered in CBM deoxygenation.<sup>49,56,57</sup>

CH<sub>4</sub> combustion over metal oxides catalysts is known to follow a redox mechanism, and a variety of kinetic models for the catalytic combustion of methane, such as the Eley–Rideal, Langmuir–Hinshelwood or Mas–van Krevelen mechanism.<sup>58,59</sup> The results of isotopic tracer experiments in Fig. 10 and 11 confirms the deoxidization reaction of CBM on LaCoO<sub>3</sub> following the Mas–van Krevelen mechanism: the lattice oxygen reacts with CH<sub>4</sub> to produce CO<sub>2</sub>, H<sub>2</sub>O and oxygen vacancies, and the surface vacancies could be replenished by bulk lattice oxygen and gas O<sub>2</sub>, which indicates the activation of O<sub>2</sub> should be a key factor for CBM deoxygenation reaction. The kinetic data in Fig. 8 also confirmed this. As shown in Fig. 14, LaCoO<sub>3</sub> could continuously provide lattice oxygen, accompanying the reduction of perovskite structure to Co/La<sub>2</sub>O<sub>3</sub>; meanwhile, O<sub>2</sub> gas could be adsorbed and dissociated on the surface, and

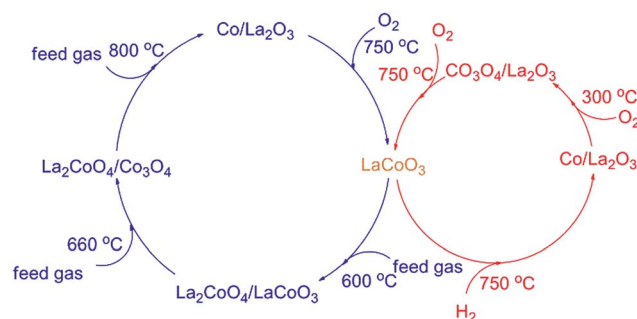


Fig. 14 The structure evolution of LaCoO<sub>3</sub> depending on the reaction gas and temperature.





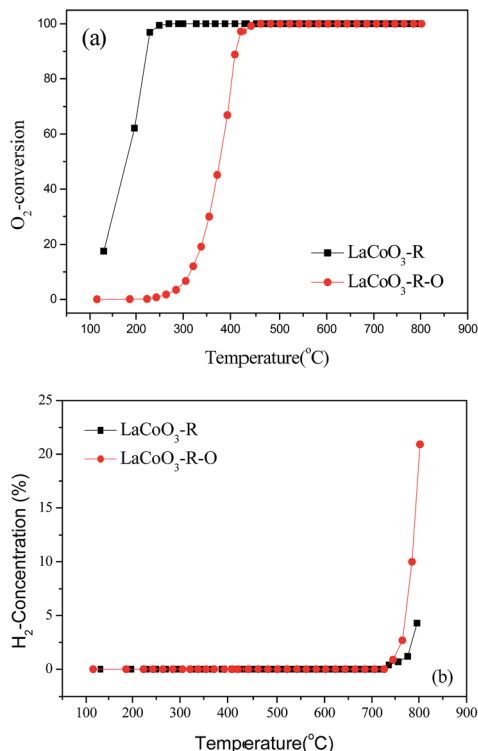


Fig. 15 The conversion of O<sub>2</sub> (a) and production of H<sub>2</sub> (b) over pre-treated LaCoO<sub>3</sub> under different conditions.

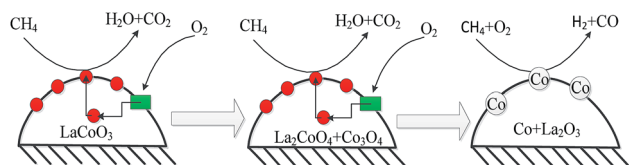


Fig. 16 CBM deoxygenation reaction on the LaCoO<sub>3</sub> catalyst (●: lattice oxygen; ■: oxygen vacancy).

incorporated into the lattice of the crystal as O<sup>2−</sup> species.<sup>60,61</sup> And therefore, the perovskite LaCoO<sub>3</sub> acted as an oxygen pump toward CBM deoxidation reaction.<sup>62</sup>

The results in Fig. 1 show the O<sub>2</sub> could be completely eliminated by CH<sub>4</sub> in the temperature range of 400 to 720 °C. As shown in Fig. 14, LaCoO<sub>3</sub> could exist as perovskite, La<sub>2</sub>CoO<sub>4</sub>/Co<sub>3</sub>O<sub>4</sub> and La<sub>2</sub>CoO<sub>4</sub>/LaCoO<sub>3</sub> in this temperature range, which indicates that the total oxidation of CH<sub>4</sub> by O<sub>2</sub> will take place on the catalyst despite the structure transformation of LaCoO<sub>3</sub> from perovskite to La<sub>2</sub>CoO<sub>4</sub>/Co<sub>3</sub>O<sub>4</sub>.

When the reaction temperature exceeds 720 °C, the CO and H<sub>2</sub> begin to form and their amounts increase significantly with continuously increasing the temperature (Fig. 1). However, the CO and H<sub>2</sub> could not be observed during the CH<sub>4</sub> pulse reaction on LaCoO<sub>3</sub> even when reaction temperature is 800 °C; the CH<sub>4</sub> pulse reaction on reduced LaCoO<sub>3</sub> (Co/La<sub>2</sub>O<sub>3</sub>) only produces CO and H<sub>2</sub> at 700 °C (Fig. 13a). Meanwhile, when Co/La<sub>2</sub>O<sub>3</sub> is partially oxidized to CoO<sub>x</sub>/La<sub>2</sub>O<sub>3</sub>, the co-existence of CoO<sub>x</sub>/La<sub>2</sub>O<sub>3</sub>

and Co/La<sub>2</sub>O<sub>3</sub> results in the formation of CO<sub>2</sub> and a significant decrease of CO/H<sub>2</sub>.

These results show the products of CBM deoxygenation reaction mainly depend on the structure of LaCoO<sub>3</sub>. When the Co species exists in an oxidised state, such as perovskite, La<sub>2</sub>CoO<sub>4</sub> or CoO<sub>x</sub>/La<sub>2</sub>O<sub>3</sub>, the CBM deoxygenation only produces CO<sub>2</sub> and H<sub>2</sub>O by the total oxidation of CH<sub>4</sub>. If Co species exists as metal, such as Co/La<sub>2</sub>O<sub>3</sub>, the preferred reaction is partial oxidation of CH<sub>4</sub>, which would lead to the formation of CO and H<sub>2</sub>.

Therefore, the CBM deoxygenation reaction on LaCoO<sub>3</sub> at different temperatures is shown schematically in Fig. 16. When the reaction temperature is below 720 °C, CH<sub>4</sub> reacts with the lattice oxygen to generate CO<sub>2</sub> and H<sub>2</sub>O despite the structure transformation from perovskite to the mixture of Co<sub>3</sub>O<sub>4</sub> and La<sub>2</sub>CoO<sub>4</sub>. With further increasing the reaction temperature, the lattice oxygen will be depleted due to the limited amount of O<sub>2</sub> in the feed gas and the perovskite structure of LaCoO<sub>3</sub> will be completely destroyed. Then, the partial oxidation of CH<sub>4</sub> could take place on the surface of metallic Co to produce by-products of CO and H<sub>2</sub>.

## 5. Conclusions

The catalyst LaCoO<sub>3</sub> prepared by the co-precipitation method exhibits high activity and catalytic stability for the CBM deoxidation reaction across a wide temperature range. The O<sub>2</sub> could be completely eliminated by CH<sub>4</sub> to produce CO<sub>2</sub> and H<sub>2</sub>O in the range of 400–720 °C, and complete deoxidation could be maintained in the temperature range of 400–660 °C for 100 h.

The perovskite LaCoO<sub>3</sub> acts as a smart catalyst during the process of CMB deoxidization; the structure of LaCoO<sub>3</sub> gradually transforms from perovskite to Co/La<sub>2</sub>O<sub>3</sub> through La<sub>2</sub>CoO<sub>4</sub>/LaCoO<sub>3</sub> and La<sub>2</sub>CoO<sub>4</sub>/Co<sub>3</sub>O<sub>4</sub> with the increasing reaction temperature, and these different structures could be transformed into each other depending on the reaction temperature and reaction gas.

When Co species exists as Co<sub>3</sub>O<sub>4</sub>, La<sub>2</sub>CoO<sub>4</sub> and/or LaCoO<sub>3</sub>, CH<sub>4</sub> is completely oxidized by O<sub>2</sub> to produce CO<sub>2</sub> and H<sub>2</sub>O. The deoxidization of CBM on catalysts follows the Mars–van Krevelen mechanism, and the activation of O<sub>2</sub> was a key factor in the deoxidization of CBM. When Co species exist as metal Co (Co/La<sub>2</sub>O<sub>3</sub>), the preferred reaction in CBM deoxygenation would be partial oxidation, which generates CO and H<sub>2</sub>. However, the complete oxidation of CH<sub>4</sub> could be recovered with the structure transformation of Co/La<sub>2</sub>O<sub>3</sub> to LaCoO<sub>3</sub> after reoxidation by O<sub>2</sub>.

## Acknowledgements

This project was supported financially by the National Key Research and Development Program of China (2016YFC0204300), the National High Technology Research and Development Program of China (2015AA034603), NSFC of China (21171055, 21333003, 21571061), the “Shu Guang” Project of the Shanghai Municipal Education Commission (12SG29), and the Commission of Science and Technology of Shanghai Municipality (15DZ1205305).



## Notes and references

- 1 L. I. Guo-jun, *Procedia Earth Planet. Sci.*, 2009, **1**, 94–99.
- 2 M. N. Debbagh, C. S. M. d. Lecea and J. Pérez-Ramírez, *Appl. Catal., B*, 2007, **70**, 335–341.
- 3 A. Olajossy, A. Gawdzik, Z. Budner and J. Dula, *Chem. Eng. Res. Des.*, 2003, **81**, 474–482.
- 4 D. Zhong and P. Englezos, *Energy Fuels*, 2012, **26**, 2098–2106.
- 5 S. Su and J. Agnew, *Fuel*, 2006, **85**, 1201–1210.
- 6 X. Guo, J. Ren, C. Xie, J. Lin and Z. Li, *Energy Convers. Manage.*, 2015, **100**, 45–55.
- 7 J. Ren, C. Xie, J.-Y. Lin and Z. Li, *Process Saf. Environ. Prot.*, 2014, **92**, 896–902.
- 8 D. W. X. C. W. Peng, Y. Z. X. Z. Keda and D. Yiyang, *Coal Conversion*, 2009, **4**, 021.
- 9 C. Ö. Karacan, F. A. Ruiz, M. Cotè and S. Phipps, *Int. J. Coal Geol.*, 2011, **86**, 121–156.
- 10 C. J. Bibler, J. S. Marshall and R. C. Pilcher, *Int. J. Coal Geol.*, 1998, **35**, 283–310.
- 11 T. Thielemann, B. Cramer and A. Schippers, *Org. Geochem.*, 2004, **35**, 1537–1549.
- 12 C. H. Bartholomew, *Appl. Catal., A*, 1993, **107**, 1–57.
- 13 C. H. Bartholomew, *Appl. Catal., A*, 2001, **212**, 17–60.
- 14 F. Yin, S. Ji, P. Wu, F. Zhao and C. Li, *J. Catal.*, 2008, **257**, 108–116.
- 15 D. Kim, S. Woo, J. Lee and O. B. Yang, *Catal. Lett.*, 2000, **70**, 35–41.
- 16 R. D. Waters, J. J. Weimer and J. E. Smith, *Catal. Lett.*, 1994, **30**, 181–188.
- 17 L. F. Liotta, G. Di Carlo, A. Longo, G. Pantaleo and A. M. Venezia, *Catal. Today*, 2008, **139**, 174–179.
- 18 A. Maione, F. André and P. Ruiz, *Appl. Catal., A*, 2007, **333**, 1–10.
- 19 T. V. Choudhary, S. Banerjee and V. R. Choudhary, *Appl. Catal., A*, 2002, **234**, 1–23.
- 20 M. Cargnello, J. J. Delgado Jaen, J. C. Hernandez Garrido, K. Bakhmutsky, T. Montini, J. J. Calvino Gamez, R. J. Gorte and P. Fornasiero, *Science*, 2012, **337**, 713–717.
- 21 A. E. York, T. Xiao and M. H. Green, *Top. Catal.*, 2003, **22**, 345–358.
- 22 Y. H. Hu and E. Ruckenstein, *Adv. Catal.*, 2004, **48**, 297–345.
- 23 S. Yang, J. N. Kondo, K. Hayashi, M. Hirano, K. Domen and H. Hosono, *Appl. Catal., A*, 2004, **277**, 239–246.
- 24 H. Y. Wang and E. Ruckenstein, *J. Catal.*, 2001, **199**, 309–317.
- 25 V. R. Choudhary, B. Prabhakar, A. M. Rajput and A. S. Mamman, *Fuel*, 1998, **77**, 1477–1481.
- 26 V. R. Choudhary, A. M. Rajput and V. H. Rane, *Catal. Lett.*, 1992, **16**, 269–272.
- 27 M. Lyubovsky, L. L. Smith, M. Castaldi, H. Karim, B. Nentwick, S. Etemad, R. LaPierre and W. C. Pfefferle, *Catal. Today*, 2003, **83**, 71–84.
- 28 Q. Zhang, X.-P. Wu, Y. Li, R. Chai, G. Zhao, C. Wang, X.-Q. Gong, Y. Liu and Y. Lu, *ACS Catal.*, 2016, **6**, 6236–6245.
- 29 Q. Zhang, Y. Li, R. Chai, G. Zhao, Y. Liu and Y. Lu, *Appl. Catal., B*, 2016, **187**, 38–248.
- 30 Q. Zhang, X.-P. Wu, G. Zhao, Y. Li, C. Wang, Y. Liu, X.-Q. Gong and Y. Lu, *Chem. Commun.*, 2015, **51**, 12613–12616.
- 31 D. Dissanayake, M. P. Rosynek, K. C. C. Kharas and J. H. Lunsford, *J. Catal.*, 1991, **132**, 117–127.
- 32 A. C. Ferreira, A. P. Gonçalves, T. A. Gasche, A. M. Ferraria, A. M. B. d. Rego, M. R. Correia, A. M. Bola and J. B. Branco, *J. Alloys Compd.*, 2010, **497**, 249–258.
- 33 B. Christian Enger, R. Lødeng and A. Holmen, *Appl. Catal., A*, 2008, **346**, 1–27.
- 34 F. F. Tao, J.-j. Shan, L. Nguyen, Z. Wang, S. Zhang, L. Zhang, Z. Wu, W. Huang, S. Zeng and P. Hu, *Nat. Commun.*, 2015, **6**, 7798.
- 35 A. J. Zarur and J. Y. Ying, *Nature*, 2000, **403**, 65–67.
- 36 L. Fabbri, A. Kryukov, S. Cappelli, G. L. Chiarello, I. Rossetti, C. Oliva and L. Forni, *J. Catal.*, 2005, **232**, 247–256.
- 37 R. Pereñíguez, V. M. González-DelaCruz, J. P. Holgado and A. Caballero, *Appl. Catal., B*, 2010, **93**, 346–353.
- 38 A. G. Bhavani, W. Y. Kim and J. S. Lee, *ACS Catal.*, 2013, **3**, 1537–1544.
- 39 K. T. C. Roseno, R. Brackmann, M. A. da Silva and M. Schmal, *Int. J. Hydrogen Energy*, 2016, **41**(40), 18178–18192.
- 40 M. R. Goldwasser, M. E. Rivas, M. L. Lugo, E. Pietri, J. Pérez-Zurita, M. L. Cubeiro, A. Griboval-Constant and G. Leclercq, *Catal. Today*, 2005, **107–108**, 106–113.
- 41 R. M. Navarro, M. C. Alvarez-Galvan, J. A. Villoria, I. D. González-Jiménez, F. Rosa and J. L. G. Fierro, *Appl. Catal., B*, 2007, **73**, 247–258.
- 42 J. Li, L. Zhao and G. Z. Lu, *Ind. Eng. Chem. Res.*, 2008, **48**, 641–646.
- 43 L. Fabbri, I. Rossetti and L. Forni, *Appl. Catal., B*, 2010, **93**, 346–353.
- 44 L. Marchetti and L. Forni, *Appl. Catal., B*, 1998, **15**, 179–187.
- 45 J. G. McCarty and H. Wise, *Catal. Today*, 1990, **8**, 231–248.
- 46 R. Lago, G. Bini, M. A. Peña and J. L. G. Fierro, *J. Catal.*, 1997, **167**, 198–209.
- 47 V. R. Choudhary, B. S. Uphade and A. A. Belhekar, *J. Catal.*, 1996, **163**, 312–318.
- 48 Å. Slagtern and U. Olsbye, *Appl. Catal., A*, 1994, **110**, 99–108.
- 49 Y. Nishihata, J. Mizuki, T. Akao, H. Tanaka, M. Uenishi, M. Kimura, T. Okamoto and N. Hamada, *Nature*, 2002, **418**, 164–167.
- 50 C. V. Schenck, J. G. Dillard and J. W. Murray, *J. Colloid Interface Sci.*, 1983, **95**, 398–409.
- 51 Z. Gao and R. Wang, *Appl. Catal., B*, 2010, **98**, 147–153.
- 52 B. Białobok, J. Trawczyński, W. Miśta and M. Zawadzki, *Appl. Catal., B*, 2007, **72**, 395–403.
- 53 J. A. Villoria, M. C. Alvarez-Galvan, S. M. Al-Zahrani, P. Palmisano, S. Specchia, V. Specchia, J. L. G. Fierro and R. M. Navarro, *Appl. Catal., B*, 2011, **105**, 276–288.
- 54 Y. Han, L. Chen, K. Ramesh, E. Widjaja, S. Chilukoti, I. Kesumawinatasurjani and J. Chen, *J. Catal.*, 2008, **253**, 261–268.
- 55 J. Xu, Y. Q. Deng, Y. Luo, W. Mao, X. J. Yang and Y. F. Han, *J. Catal.*, 2013, **300**, 225–234.



- 56 N. Guilhaume, S. D. Peter and M. Primet, *Appl. Catal., B*, 1996, **10**, 325–344.
- 57 H. Tanaka, I. Tan, M. Uenishi, M. Taniguchi, M. Kimura, Y. Nishihata and J. i. Mizuki, *J. Alloys Compd.*, 2006, **408–412**, 1071–1077.
- 58 N. Bahlawane, *Appl. Catal., B*, 2006, **67**, 168–176.
- 59 V. Belessi, A. Ladavos, G. Armatas and P. Pomonis, *Phys. Chem. Chem. Phys.*, 2001, **3**, 3856–3862.
- 60 S. Royer, H. Alamdari, D. Duprez and S. Kaliaguine, *Appl. Catal., B*, 2005, **58**, 273–288.
- 61 G. Saracco, G. Scibilia, A. Iannibello and G. Baldi, *Appl. Catal., B*, 1996, **8**, 229–244.
- 62 R. Hammami, S. B. Aïssa and H. Batis, *Appl. Catal., A*, 2009, **353**, 145–153.

